HHS Public Access

Author manuscript

J Neural Eng. Author manuscript; available in PMC 2016 October 01.

Published in final edited form as:

J Neural Eng. 2015 October ; 12(5): 056017. doi:10.1088/1741-2560/12/5/056017.

Hippocampal Closed-Loop Modeling and Implications for Seizure Stimulation Design

Roman A. Sandler[*,1], **Dong Song**[1], **Robert E. Hampson**[2], **Sam A. Deadwyler**[2], **Theodore W. Berger**[1], and **Vasilis Z. Marmarelis**[1]

[1]Department of Biomedical Engineering, University of Southern California, Los Angeles, CA, USA

[2]Department of Physiology & Pharmacology, Wake Forest University, Winston-Salem, NC, USA

Abstract

Objective—Traditional hippocampal modeling has focused on the series of feedforward synapses known as the trisynaptic pathway. However, feedback connections from CA1 back to the hippocampus through the Entorhinal Cortex (EC) actually make the hippocampus a closed-loop system. By constructing a functional closed-loop model of the hippocampus, one may learn how both physiological and epileptic oscillations emerge and design efficient neurostimulation patterns to abate such oscillations.

Approach—Point process input-output models where estimated from recorded rodent hippocampal data to describe the nonlinear dynamical transformation from CA3→CA1, via the Schaffer-Collateral synapse, and CA1→CA3 via the EC. Each Volterra-like subsystem was composed of linear dynamics (Principal Dynamic Modes) followed by static nonlinearities. The two subsystems were then wired together to produce the full closed-loop model of the hippocampus.

Main Results—Closed-loop connectivity was found to be necessary for the emergence of theta resonances as seen in recorded data, thus validating the model. The model was then used to identify frequency parameters for the design of neurostimulation patterns to abate seizures.

Significance—DBS is a new and promising therapy for intractable seizures. Currently, there is no efficient way to determine optimal frequency parameters for DBS, or even whether periodic or broadband stimuli are optimal. Data-based computational models have the potential to be used as a testbed for designing optimal DBS patterns for individual patients. However, in order for these models to be successful they must incorporate the complex closed-loop structure of the seizure focus. This study serves as a proof-of-concept of using such models to design efficient personalized DBS patterns for epilepsy.

1 Introduction

The hippocampus is amongst the most studied of brain regions and has been implicated extensively in physiological functions of learning and memory as well as pathologies such as Alzheimer's disease and Epilepsy. Traditionally, information processing through the

[*]Corresponding Author: rsandler00@gmail.com.

hippocampus has been viewed in the context of the trisynaptic pathway, a series of feedforward synapses from the entorhinal cortex (EC) through the Dentate Gyrus and area CA3 to area CA1. However, there has long been evidence to support the notion that CA1 may also causally influence CA3 (see Fig. 1). Deadwyler et al. (1975) was the first to show that population spikes from the hippocampus may reenter the hippocampus via the EC, thus giving the first physiological evidence of a functioning hippocampal-entorhinal loop. Since then, multiple anatomical and physiological studies have elucidated the complex interconnected nested-loop nature of the hippocampal-entorhinal formation (Finch et al., 1986; Buzsáki, 1989; Tamamaki and Nojyo, 1995; Iijima et al., 1996; Kloosterman et al., 2004; Bartesaghi et al., 2006). Our group has recently shown that there exists a significant predictive relationship between single neurons from area CA1 to area CA3 in the rodent hippocampus (Sandler et al., 2014). Furthermore, many studies have proposed the hippocampal-entorhinal loop may serve as the anatomical substrate for the uncontrolled network oscillations which characterize seizures (Pare et al., 1992; Stringer and Lothman, 1992; Nagao et al., 1996; Barbarosie and Avoli, 1997; Boido et al., 2014). Finally, the hippocampal-entorhinal loop has been suggested to support the sort of reverberatory activity which has been theorized to be necessary for working memory, a well-known function of the hippocampus (Hebb, 1949; Fuster, 2000; Kloosterman et al., 2004)

Past work by our group has led to the development of several nonlinear nonparametric predictive models of the transformation of action potential activity from the CA3 to the CA1 region of the rodent hippocampus (Song et al., 2007; Zanos et al., 2008; Song et al., 2009a; Marmarelis et al., 2009; Sandler et al., 2015). Most recently, we have utilized the concept of Principal Dynamic Modes (PDMs) to achieve a more compact representation of our model and to facilitate its physiological interpretation (Marmarelis et al., 2013a, 2014; Sandler and Marmarelis, in press). These ‘open-loop’ models have been validated both computationally and experimentally in the context of hippocampal neuroprosthetics (Song et al., 2007; Berger et al., 2012; Hampson et al., 2012).

Although much attention has been given to quantitatively understanding the CA3→CA1 dynamical transformation, almost no work has been done to quantitatively understand the CA1→CA3 dynamical transformation and the resulting hippocampal closed-loop. Here we propose a nonparametric closed-loop point-process (CLPP) model of the hippocampal-entorhinal formation. The closed-loop model is composed of two bidirectionally connected ‘open-loop’ PDM-based subsystems which model the nonlinear dynamical transformation from CA3→CA1 and CA1→CA3. The purpose of the closed-loop model is not to accurately predict the output time-series, as is the case with the aforementioned open-loop models, but rather to study the phenomena which emerge from the closed-loop network configuration. For example, the response of the system to external perturbation involves not only the feedforward transformation from CA3→CA1, but also to loop effects arising from the CA1→CA3 feedback connection. Thus, even a highly predictive open-loop model may prove misleading when examining this issue due to its lack of feedback connectivity.

Once the closed-loop system is estimated from real hippocampal data, it is used to model ‘in-silico’ the effects of externally stimulating imposed the hippocampal-entorhinal system with arbitrarily designed stimulation patterns. It was found that under broadband (Poisson)

stimulation, theta resonant modes emerged only in the closed-loop system, and not in the open loop system, suggesting that closed-loop connectivity is essential for strong network oscillations to occur. The response of the system was then analyzed for random narrowband spike trains of various frequencies. It was found that high-theta/low-alpha stimulation (6-14 Hz) greatly increased output activity, while delta (<5 Hz) and low gamma (30 Hz) significantly reduced it. We suggest that such a model may prove useful in designing efficient neurostimulation patterns which aim to abate the uncontrolled network oscillations which characterize seizures. Some of these results were presented previously in the form of a conference paper (Sandler et al., 2013).

2 Methods

2.1 Experimental Protocols & Data Preprocessing

A Male Long-Evans rat was trained to criterion on a two lever, spatial Delayed-NonMatch-to-Sample (DNMS) task. Spike trains were recorded in-vivo with multi-electrode arrays implanted in the CA3 and CA1 regions of the hippocampus during performance of the task. These experiments were conducted in the labs of Dr. Deadwyler and Dr. Hampson at Wake-Forest University and have been described in detail in our previous publications (Hampson et al., 2012). Only neural activity from trials where the rat successfully completed the DNMS task was used. Spikes were sorted, time-stamped, and discretized using a 12 ms bin. Spike train data from 1s before to 3s after the sample presentation phase of the DNMS task was extracted and concatenated into one time series.

2.2 Closed-Loop Point-Process (CLPP) Model

The closed-loop model of the reciprocal relation between the CA1 and CA3 regions is configured as shown in Fig. 1e. It involves two input-output PDM-based subsystems, CA3→CA1 and CA1→CA3, (see section 2.3 below) which are reciprocally connected. It also involves two external disturbances, e1 and e3, that are the model-prediction residuals of the two input-output models. These disturbances correspond to the exogenous inputs to the closed-loop model that are not accounted for by the two input-output subsystems.

Thus, e1 represents all non-CA3 inputs to CA1, such as the direct pathway from EC to CA1 (Yeckel and Berger, 1990; Jones, 1993). Likewise, e3 represents inputs entering the system between CA1 and CA3 – e.g. from the prefrontal cortex and septum (Buzsáki, 1996; Colom, 2006). These external disturbances combine with the respective subsystem outputs, CA1p and CA3p, to form the inputs for the subsequent subsystem, CA1m and CA3m. Note that physiologically, CA3p and CA1p, the subsystem outputs, correspond to the spike activity in CA3 and CA1 which is caused by feedback connections from CA1 and CA3, respectively. Thus, CA3m and CA1m, being the sum of feedback and exogenous spikes, correspond to the spike train signals one would measure experimentally. Essentially, our model decomposes the recorded CA3/CA1 activity into endogenous activity arising from the closed-loop nonlinear dynamics (CA3p and CA1p) and exogenous activity arising from external inputs (e3 and e1). Thus, once the CLPP model is estimated from real data, it can be stimulated with any arbitrary exogenous signals, while preserving the endogenous dynamics.

In the beginning of each simulation, all of the signals were initialized based on real data, and then CA3m was fed through the CA3→CA1 subsystem to obtain an updated value for CA1p. Then, in order to 'skip-ahead', or move up one time step each iteration, the last element of the updated CA1p was concatenated onto the previous CA1p signal This process was then repeated for each iteration of the simulation.

To see which results arise purely from the closed-loop structure of our model, as opposed to the nonlinear dynamics of either of the component subsystems, an open-loop model, as shown in Fig. 2, was also analyzed. In the open-loop model, the connections between the two subsystems were severed, such that stimulating the open-loop model is equivalent to stimulating both subsystems in isolation.

2.3 Feedforward Input-Output Models

Two Volterra-like PDM models (see Fig.3 were used to describe the spike train transformations from CA3 to CA1 (via the Schaffer collateral pathway) and from CA1 to CA3 (via the subiculum, entorhinal cortex, and dendate gyrus) (Marmarelis et al., 2013a). In the PDM-based model, the input signal is first convolved with L linear filters (the PDMs) and the PDM outputs are transformed through static nonlinearities, termed the Associated Nonlinear Functions (ANFs). The sum of the ANF outputs is fed into a Threshold -Trigger operator that generates an output spike if its input exceeds a fixed threshold value. The PDMs can be understood as a system-specific basis of functions that efficiently describe the system dynamics. The ANFs represent the conditional probability of an output spike given a specific PDM input value and can be viewed as 'link functions' connecting a given PDM with the pre-threshold output. Thus, PDMs with larger amplitude ANFs make more significant contributions to the output. Input-output spike data were used to estimate all parts of the model with methods previously reported (Marmarelis et al., 2013a).

For the same input, the CLPP system will generate a much higher MFR output than its open-loop correlate. This occurs due to the binary nature of the CLPP system; namely, the subsystems may only have excitatory outputs (ie 'positive' spikes) and not inhibitory outputs (ie negative spikes). Thus, in closed-loop mode, the input to each subsystem will not only be the exogenous input, but also additional spikes from the other subsystem, which will lead to more spikes in the output. In order to maintain signals with physiologically plausible MFRs, the thresholds of the subsystems were raised relative to open-loop conditions. The open-loop 'reference' threshold was calculated to maximize true positive spikes while minimizing false negative spikes according to the methods defined previously in Marmarelis et al. (2013a).

The predictive power of the models was visualized using Receiver Operating Characteristic (ROC) curves, which plot the true positive rate against the false positive rate over the putative range of threshold values for the continuous output, y (Zanos et al., 2008). The area under the curve (AUC) of the ROC plots was used as a performance metric of the models, and has been shown to be equivalent to the Mann-Whitney two sample statistic (Hanley and McNeil, 1982). The AUC ranges from 0 to 1, with 0.5 indicating a random predictor and higher values indicating better model performance. The AUC metric was chosen as it measures the similarity between a continuous 'prethreshold' signal and a spike train, thus allowing us to avoid the somewhat arbitrary process of choosing a threshold trigger value.

Monte Carlo simulations were used to test the null hypothesis that the given CA3 (or CA1) neuron can predict the output CA1 (or CA3) neuron's spiketimes significantly better than a random neuron of the same MFR (see Sandler et al. (2014) for more info). If the null hypotheses could be rejected with > 99% confidence, we can conclude that the two neurons under question are indeed bidirectionally connected, thus warranting closed-loop analysis.

In the Volterra-PDM model, the domain of each ANF is limited by the power of the input used to estimate the model. This can be seen by examining the domain of each ANF, which spans a finite interval whose endpoints are determined by the maximum/minimum value of its respective PDM input. This presents a problem in the CLPP model, where at each iteration the Volterra-PDM subsystems are fed a new input which cannot be predicted at the outset of the simulation. Thus, there exists the possibility that the PDM outputs / ANF inputs will exceed the domain of the ANFs, and thus the domain of the Volterra-PDM subsystem. To overcome this issue, the ANFs were extended in both directions by the mean of their last two endpoints.

In order to examine the emergent properties of CLPP systems, ‘barebones’ synthetic systems were also analyzed where ‘ground truth’ was available. These systems reduced the complexity of a full Volterra-PDM system by (1) excluding ANFs, making the threshold trigger the only nonlinearity, (2) Having only one PDM, and (3) having the two subsystems of the CLPP system to be equivalent.

2.4 Random Narrowband Spike-Train Generation

To generate random narrowband (RNB) spike-train disturbances centered around a given frequency, f_0, the following algorithm was used: first, a broadband (Poisson) spike train with a given MFR was generated. Then the spike train was filtered through a butterworth bandpass filter with a passband of 4 Hz centered around f_0. The filter output (a continuous signal) was then thresholded to generate the final narrowband spike train. The threshold value was selected such that the MFR of the output narrowband spike trains was equivalent to that of the original broadband spike train. An example of a narrowband spike train is shown in Fig. 2.4b (top row). Note that unlike classical linear filters, the harmonics of f_0 will also appear to varying degrees due to the nonlinearity of the threshold operator. To our knowledge, this useful and efficient method of attaining narrowband spike trains has not been previously discussed in the literature.

3 Results

3.1 Estimated Volterra-PDM subsystems

The estimated Volterra-PDM subsystems for CA3→CA1 and CA1→CA3 appear in Fig. 4. It was found that a set of 3 PDMs (with 3 corresponding ANFs and a threshold value) is sufficient for each input-output subsystem. The ROC plots shown in Fig. 5A indicate that both models have roughly the same predictive capability. Furthermore, using Monte Carlo simulations, it was found that both neurons are indeed bidirectionally connected ($P < .0001$ in both cases, see Fig. 5B,C). This result is corroborated by our previous study where it was found that the CA1→CA3 predictive power was roughly equivalent to the CA3→CA1

predictive power (Sandler et al., 2014). Although this result may seem surprising given the greater number of synapses and exogenous inputs going from CA1 to CA3, as compared to going from CA3 to CA1, it should be noted that anatomical connectivity is only one aspect of predictive power, which is also influenced by connection 'impact' and unobserved inputs (see section 4.2). We note that the frequency-domain representations of the PDMs exhibit spectral peaks in the theta (4-8 Hz) and delta (<4 Hz) bands. These peaks were found to be critical in defining the resonant characteristics of the closed-loop model. Similar results linking the PDM spectral peaks with the celebrated cerebral rhythms were previously obtained in the primate neocortex (Marmarelis et al., 2013a, 2014).

3.2 Stimulation with Model Prediction Residuals

In order to better illustrate the role of the disturbances and intraloop signals in the CLPP model, model prediction residuals were first used to stimulate the estimated CLPP system. The residuals were defined as:

$$e_3 = CA3 - CA3_p \quad (1)$$

$$e_1 = CA1 - CA1_p \quad (2)$$

where CA3/CA1 are the actual recorded spike trains and CA3p/CA1p are the subsystem predictions. The results are shown in Fig. 6. In this formulation the Volterra-PDM subsystems capture the essential endogenous nonlinear dynamics between the two neurons, while the residuals represent exogenous disturbances that drive the CLPP system. It should be noted that e3 and e1 are tertiary signals, with 1 indicating a false negative and −1 indicating a false positive in the model predictions. Physiologically, the −1 values are viewed as exogenous inhibitory signals which prevent an output spike. Since in this case the exogenous inputs are the open-loop residuals, the measured signals (CA3m and CA1m) are by definition equivalent to the recorded signals CA3p and CA1p.

3.3 Stimulation with Random Poisson Inputs

The operation of the CLPP model can be stimulated with any chosen external disturbances, and not just the empirical residuals (as done above), to examine its response characteristics. Here, the spectral characteristics of the CLPP model were examined through stimulation with two independent random broadband (Poisson) disturbances. The resulting CLPP intra-loop spike trains (shown in Fig. 7) were found to exhibit theta band oscillations, which were present in our recorded CA3 spike train and are known to be prevalent in the rodent hippocampus (Buzsáki, 2002; Colgin, 2013). The thresholds of the CLPP subsystems were chosen as to minimize theta resonances in CA1 while maintaining them in CA3, as was observed in real data (see section 3.4). It should be emphasized that these resonant modes emerge purely from the nonlinear dynamical nature of our model and not through any of the inputs, which are broadband.

To distinguish whether the emergent resonant modes arise from any of the individual subsystems or from the closed-loop configuration of our model (e.g. the specific connectivity of the two subsystems) the open-loop version of our model (Fig. 2) was stimulated using the same broadband spike trains. The results, shown in Fig. 8, show that while the open-loop model can produce very weak theta oscillations, only the full closed loop model can produce the strong theta, and to a lower extend delta, oscillations shown in actual CA3 recordings. The fact that strong theta and delta oscillations are an emergent characteristic of the closed-loop model of the hippocampus, and not the open-loop model, represents a key finding of our study and constitutes a means of validating the CLPP model and its potential utility.

In order to examine how the specific characteristics of the resonant modes emerge from the Volterra-PDM subsystems, simple 'barebones' synthetic subsystems were analyzed (see methods). A CLPP system was constructed where both subsystems were identical and consisted only of a single PDM and a threshold trigger (without an ANF). The single PDM, shown in Fig. 9a, consisted of a cosine function of frequency, f_0. When this system was stimulated with Poisson spike trains, the CLPP output signals (CA3m, CA1m) were found to have resonant modes exactly at the PDM frequency f_0 (Fig. 9b). Furthermore, if the PDM had no resonant peak, there were no corresponding resonant peaks in the CLPP output signals (results not shown). These results, which were obtained over several values of f_0 (Fig. 9c), show that the emergent resonant modes are intimately linked to the PDM spectral peaks, which represent the unique dynamical properties of each subsystem.

It should be noted that a well established result of linear systems theory states that the output of a linear system in the frequency domain is the product of the system transfer function and the input in the frequency domain ($Y(w) = H(w)*X(w)$). Our result extends the essence of this result to spike train systems where the output goes through a highly nonlinear thresholding operation (Marmarelis et al., 1986). Empirically, the main difference of our point-process system and linear systems is the addition of harmonics caused by the thresholding operation. In the synthetic cosine system, these harmonics are odd-integer multiples of f_0 and can be seen in Fig. 9b,c. It should be noted that such harmonics have been observed in electrophysiological experiments (Leung and Yu, 1998).

3.4 Affect of Trigger Threshold on Resonant Modes

Several researchers have pointed out that the baseline and threshold potential in individual neurons and neuronal populations are not static but rather both dynamical, varying with the neuron's past spiking activity, and nonstationary, varying over time due to a variety of external factors (Lu et al., 2012). Furthermore, it has been shown that the baseline potential is significant for the development of spontaneous cellular oscillations such as theta (Fricker et al., 1999). In our subsystem models, the baseline potential and threshold potential are both encapsulated in the threshold trigger. The CLPP output resonant mode power was calculated for identical broadband inputs over several values of the threshold trigger parameters of both subsystems, as shown in Fig. 10. Threshold values were presented as percentage deviations from the reference threshold value, which was defined in section 2.3. It can be seen that the threshold value can either facilitate or inhibit the emergent theta resonant mode in either

subsystem. Furthermore, the same threshold value can affect CA3 and CA1 differently. This modulating effect of thresholds on resonant modes is significant as it could help account for the fact that in actual data, the theta mode is present only in CA3, not CA1.

To more accurately study the effects of the threshold trigger on the emergent resonant modes, we analyzed a simple 'barebones' synthetic system identical to that of the previous section. The only difference was that the single PDM was the sum of two cosine waves of different frequencies f_1 and f_2, as shown if Fig. 11a (time-domain) and 11b (frequency domain). The synthetic CLPP system was stimulated with identical broadband signals over several values of the threshold trigger. For each simulation, the power in the $f_1 = 2Hz$ and $f_2 = 7Hz$ frequencies was calculated in the output signals. It was observed that each simulation had only one dominant resonant mode which was determined by the threshold trigger value (Fig. 11c,d). Thus when the threshold was set to 4, f_1 was dominant while f_2 was almost entirely unobserved (Fig. 11e), but when the threshold was set to 5, the roles were reversed with f_2 dominant and f1 unobserved (Fig. 11f). This synthetic study confirms the role of the threshold in tandem with the PDMs to determine the characteristics of the output resonant modes. This unique role of the threshold in determining which resonant modes will emerge in the system has no correlate in linear systems theory.

3.5 Stimulation Testing

An advantage of closed-loop modeling relative to open-loop modeling is that it may provide a more accurate prediction of the system response to external perturbation due to its incorporation of feedback components (Marmarelis et al., 2013b). Understanding the hippocampal response to stimulation is vital for designing effective neurostimulation patterns for seizure abatement in the emerging field of deep-brain stimulation for epilepsy (see section 4.4). The response characteristics of the CLPP model for two random narrowband (RNB) disturbances of various oscillation frequencies were examined. Each RNB disturbance was constructed according to the procedure defined in section 2.4. It should be noted that while the RNB signals had different frequencies of oscillation, their *mean* firing rate (MFR) was the same - i.e. they had the same amount of spikes. This is essential, since the pulsecount of periodic, or fixed-interval, stimuli is directly proportional to their frequency. Thus, it is impossible to disentangle whether a given stimulus performs better due to its frequency or due to its spikecount.

The MFR of the intra-loop CA1 activity is plotted in Fig. 12a for various oscillation frequencies of the two RNB disturbances (x-axis is for e3 and y-axis is for e1). Increase of CA1 activity is observed when either e3 or e1 were stimulated in the theta/alpha range (6-14 Hz). Highest increase is seen for the combination of theta stimulation in e3 and alpha stimulation in e1. Most intriguing is the finding that the combination of low-gamma stimulation (28-30 Hz) in both disturbances, as well as high-delta stimulation (4-5 Hz) in e1, results in significant suppression of CA1 activity (Fig. 12b).

In order to further disentangle the contributions of the individual subsystems and the closed-loop configuration to the CLPP frequency response, a single-input closed-loop system was constructed which had only one disturbance signal: e3 (Fig. 13a). e3 was chosen over e1 since presumably much more exogenous inputs enter the system from CA1 to CA3, via the

EC, rather than the direct pathway from CA3 to CA1. The threshold of the single-input systems was set such that when it is stimulated with the recorded CA3 signal, the output CA1 MFR is equivalent to the recorded CA1 MFR. Identical RNB disturbances where then used to stimulate both the single-input closed-loop system and the open loop CA3→CA1 system (Fig. 2). The output MFR for each RNB frequency, shown in Fig. 13b, can be understood as "point-process transfer functions", analogous to the transfer function studied in linear systems. The differences between the responses' of the two systems quantitatively measures how the CA1→CA3 feedback connectivity strengthens/ attenuates various input frequencies. For example, while both open-loop and closed-loop systems respond strongly to theta and suppress activity above 18 Hz, the closed-loop system strongly amplifies the open-loop theta response. This helps explain why a full closed-loop model is needed to replicate the strong theta oscillations seen in empirical data (Fig. 8) Furthermore, the resonant theta frequency is raised from 4 Hz in the open-loop case to 8 Hz in the closed-loop case.

Several groups have shown experimental evidence that random Poisson stimulation can be more efficacious for seizure abatement than periodic stimulation (Wyckhuys et al., 2010; Van Nieuwenhuyse et al., 2014; Buffel et al., 2014). Here, the CLPP system was used as a testbed to assess the efficacy of oscillatory vs random stimulation. Namely, the system was stimulated with oscillatory RNB spiketrains and broadband/random Poisson spiketrains of increasing MFRs. To allow fair comparison, for each frequency, the total spikecount of the RNB trains matched the spikecount of the Poisson spiketrains. Thus, unlike in Fig 12 where the spikecount of the RNB was kept constant, here both the frequency and spikecount of the RNB trains progressively increased. To maintain simplicity, only CA3 was stimulated, as in the single-input CLPP system of Fig. 13a. As shown in Fig. 14, the response of increasing the MFR of Poisson trains was simple: more input spikes meant more output spikes. The response of the RNB train, however was more complex. Once again the theta resonance peak can be seen, along with inhibition from 15-30 Hz. These results suggest that oscillatory vs random is not the correct question to ask, as the answer depends will vary depending on which frequency is used. Rather, one should ask what is the optimal frequency of stimulation. It should be noted that these results for RNB stimulus cannot be compared with Fig. 12,13, since as already mentioned, there the MFR was kept constant, while here it is progressively increasing to match the Poisson MFR.

4 Discussion

This paper present a methodology for closed-loop modeling of the hippocampal CA3 and CA1 regions. The model is composed of two PDM/ANF subsystems followed by a threshold trigger as described in our previous publications (Marmarelis, 2004; Marmarelis et al., 2013a). The PDMs can be thought of as an efficient basis of functions to describe the dynamical transformation between any two signals, while the ANFs describe the static nonlinearity which 'links' the PDM output with the output spike train. The PDM/ANF methodology for modeling nonlinear systems has shown itself to be a highly robust and flexible method which lends itself to physiological interpretation. Stimulation of the closed-loop model showed the emergence of theta oscillations, a phenomena not seen in the open loop models. Also, simulation of the closed-loop model with RNB stimulation suggests that our model can be useful in optimizing neurostimulation patterns to suppress seizures.

4.1 Closed-Loop Modeling

Closed-loop modeling is to be used whenever two signals bidirectionally influence each other. Although the data used in this study was from the CA3 and CA1 regions of the hippocampus, in principle the model can be used for any bidirectionally causal point-process signals. A similar model based on continuous signals was previously used to model cerebral hemodynamics (Marmarelis et al., 2013b). There, the response of the system to perturbations of blood pressure and CO_2 was compared in open-loop and closed-loop mode. Here, closed-loop modeling was used due to the complex nested-loop nature of hippocampal anatomy and several experimental studies which have confirmed that electrical activity can reenter and reverberate through the hippocampal-entorhinal formation (see Fig. 1 and section 4.2.

Traditional model validation criteria such as those measuring predictive power cannot be applied to the closed-loop model since it does not aim to predict an output spike train as open-loop models usually do; rather it aims to describe the behavior of the system under various external stimuli. We suggest that the emergence of theta resonances in the closed-loop model and not in the open-loop models provides validation and utility to the closed-loop model (see Fig. 8). One approach to rigourously validate the closed-loop model would be to stimulate the system and compare the system response with the open-loop and closed-loop model predictions such as those shown in Fig. 13 and 8. Such data, however, was not available in this study.

It is important to clarify the distinct roles of open-loop and closed-loop modeling. Open-loop models, such as those derived previously for the hippocampus (Song et al., 2007; Zanos et al., 2008; Marmarelis et al., 2013a), aim to describe the functional transformation of activity from CA3 to CA1, or vice-versa. However, open-loop modeling will be misleading when describing phenomena which involve the entire closed-loop system. A notable example of this is the response of the system to external perturbations as these perturbations will not only affect the target area but will reverberate around the entire loop. This is why the open-loop model was not able to predict the emergence of theta resonances in response to external broadband stimulation. Knowing how the hippocampus responds to external stimulation is particularly important for the emerging field of deep-brain stimulation which aims to use precisely such stimulation to abate seizures, which are characterized by hypersynchronous resonant activity (see section 4.4).

It should be noted that closed-loop modeling is different from the more commonly used autoregressive modeling such as done in Song et al. (2007); Eikenberry and Marmarelis (2013); Valenza et al. (2013). In autoregressive modeling, the output time-series past has an effect on the output present. In closed-loop modeling, the output time-series past has an effect on the *input* present. In practice, this subtle difference means that during simulations, the input to a given subsystem must continuously be reevaluated as it evolves through the simulation. In future work it would be beneficial to develop a nested-loop model which incorporates both closed-loop effects that model hippocampal reentrance and autoregressive effects that model the neural refractory period and afterhyperpolarization, a feature absent from our current model (Spruston and McBain, 2007).

4.2 Hippocampal Reentrance

The closed-loop model is based on the working hypothesis that CA1 can causally influence CA3. Anatomically, this may arise through backprojecting interneurons from CA1 to CA3 (Sik et al., 1994), or through the hippocampal-entorhinal loop (Fig. 1a). Deadwyler et al. (1975) was the first to show that population spikes induced in CA3 spread to the EC and reentered CA3 through the Dendate Gyrus. Since then, several studies have used local field potential (LFP) recordings to confirm reentrance and to elucidate the multiple simultaneous anatomical pathways by which it may occur. It has been shown that reentrant activity may leave the hippocampus either directly from CA1→EC or from CA1→Subiculum→EC (Finch et al., 1986; Tamamaki and Nojyo, 1995; Craig and Commins, 2005). Furthermore, activity may reenter the hippocampus either through the Dendate Gyrus or CA3 via the perforant path (Stringer and Lothman, 1992; Wu et al., 1998; Kloosterman et al., 2004) or directly from EC→CA1 via the temporoammonic path (Yeckel and Berger, 1990; Jones, 1993; Bartesaghi and Gessi, 2003). Optical imaging studies have also clearly shown that information can reenter and reverberate around the hippocampal-entorhinal loop (Iijima et al., 1996; Ezrokhi et al., 2001). An advantage of the data-driven nonparametric modeling approach used here is that no *a priori* assumptions are made about the system under study, and thus reentrance can be modeled without complete knowledge of its underlying pathways and mechanisms. Furthermore, the model will not change with future physiological discoveries (Marmarelis, 2004; Song et al., 2009b,c).

Most studies on reentrance have analyzed LFP activity induced by electrical stimulation. In a previous paper, we have used a large dataset of neurons to demonstrate predictive power (ie Granger causality) from CA1 to CA3 on the single-neuron level in the nonpathological unperturbed brain. There it was found that of the 144 neuron pairs examined, 96 (67%) showed CA1→CA3 causality. Furthermore, it was found that the number of bidirectionally connected neurons was significantly higher than would be expected by chance, suggesting the CA3 and CA1 pyramidal cells tend to be wired topographically in a bidirectional/loop fashion. This finding has also been confirmed experimentally in both anatomical and physiological studies (Tamamaki and Nojyo, 1995; Buzsáki, 1989). Although much evidence points to true causality from CA1→CA3 on the network (LFP) level, and the previous paper showed Granger causality on the single neuron level, the extent of true causality on the single neuron level has yet to be established due to possibility of unobserved inputs such as the septum influencing both CA3 and CA1 regions (Colom, 2006). Thus, the results of this study must be regarded with some caution until experiments will be performed which elucidate the relative influence of truly causal connections and unobserved inputs on the CA1→CA3 predictive relationship.

4.3 Theta Emergence

Hippocampal theta rhythms have been extensively studied and implicated in neural coding, learning, and memory (for excellent reviews, see Buzsáki (2002); Axmacher et al. (2006); Colgin (2013); Buzsáki and Moser (2013)). The mechanisms by which network theta oscillations emerge in the hippocampus involve complex interactions occurring simultaneously on many hierarchal levels. On a cellular level, EC stellate cells and hippocampal pyramidal cells have been shown to have inherent membrane resonances in the

theta range (Leung and Yu, 1998; Pike et al., 2000; Haas and White, 2002; Schreiber et al., 2004). On a regional level, CA1, CA3, and the EC have been shown to generate theta oscillations endogenously in-vivo (Alonso and Garcia-Austt, 1987; Kocsis et al., 1999; Goutagny et al., 2009). Although cellular membrane resonances cannot by themselves lead to theta oscillations, they have been theorized to strongly influence frequency of oscillation in networks of interconnected pyramidal cells and interneurons such as those found in the above 'pacemaker' areas (Hutcheon and Yarom, 2000). Finally, on the interregional level, the above pacemakers are interconnected in a complex nested loop and receive inputs from the medial septum (Fig. 1a), which has been shown to be critical for the emergence of hippocampal theta (Winson, 1978; Colom, 2006).

In the present model we have shown that neuronal theta oscillations emerge through the closed-loop modeling of the hippocampal-entorhinal formation; furthermore, these rhythms are absent in the open-loop configuration. Although the model was based on recordings of CA3 and CA1, the nonparametric data-driven nature of the PDM modeling approach implies that several hierarchal levels of interaction will be incorporated into the PDMs. For example, CA3→CA1 PDMs incorporate both CA1 neuronal integration (a cellular mechanism) and potential CA1 pyramidal-interneuron interactions (a regional mechanism). Because it is not yet clear how much the PDMs are influenced by unobserved inputs (see section 4.2), the current results must be regarded with caution. At the very least, we have shown that although open-loop systems may show a slight preference for theta, closed-loop modeling and bidirectional connectivity is necessary for full neural oscillations to emerge (see Fig. 8). This is well supported by experiments which have shown CA1 to be an endogenous theta generator but have not shown any theta resonances in responde to white noise stimulation (Jahnsen and Karnup, 1994; Goutagny et al., 2009). Furthermore, we have provided strong evidence to support the hypothesis that the hippocampal-Entorhinal loop is involved in generating and modulating hippocampal-entorhinal theta rhythms. However, the full extent of this involvement can only be clarified once the causality question is resolved.

4.4 Epilepsy and Seizure Abatement

Epilepsy is a neurological disorder characterized by chronic seizures which affects 1-2% of the US population (Begley et al., 2000). Although the mechanisms of seizure development are still not clear, several animal studies have linked hippocampal ictal activity with uncontrolled oscillations along the hippocampal-entorhinal loop (Pare et al., 1992; Stringer and Lothman, 1992; Nagao et al., 1996). Interestingly, a study by Barbarosie and Avoli (1997) showed that 1 Hz stimulation of CA1 actually decreased seizure frequency along the hippocampal-entorhinal loop. This finding is also reflected in our results where it was found that <2 Hz stimulation decreased output activity (see Fig. 12). Later a study by Bragin et al. (1997) showed that in-vivo ictal activity could emerge independently in both the EC and hippocampus even after the two were lesioned. This supported the notion that seizure rhythmicity was due to a complex coupling of nested oscillators rather than just a single closed loop oscillator. Although the role of the hippocampal-entorhinal loop in human temporal lobe epilepsy (TLE) remains unknown, these animal studies suggest that it is intimately involved in initiating and sustaining seizures and that perturbation of this loop with electrical stimulation may abate seizure onset.

Deep brain stimulation (DBS) is a promising new alternative to traditional epilepsy treatments such as antiepileptic drugs and resective surgery which both have major drawbacks: drugs have a 30% nonresponder rate and strong side-effects, while surgery isn't applicable for all patients, has acute and long-term risks, and has a large remission rate (Brodie and Dichter, 1996; Engel et al., 2003). Responsive cortical focal stimulation has recently been approved in the US and scheduled thalamic stimulation has previously been approved in Europe (Ben-Menachem and Krauss, 2014; Heck et al., 2014; Fisher and Velasco, 2014). However the mechanisms by which DBS works are still not clear and few quantitative models have been developed (Durand and Bikson, 2001; Mina et al., 2013). The above studies suggest that a better understanding of hippocampal-entorhinal loop dynamics may help elucidate the mechanisms by which DBS abates temporal lobe seizures. Furthermore, a computational model of these dynamics may not only serve to elucidate these mechanisms, but also assist in designing efficient neurostimulation patterns, a process currently done by physicians using a brute-force approach. Such a framework has recently been applied for designing efficient DBS patterns for epilepsy (Taylor et al., 2015) and Parkinson's disease (Holt and Netoff, 2014; Grill et al., 2014). However, in Parkinson's disease the barriers to clinical translation are much lower since stimulation efficacy can be assessed intermediately by observing the change in patient tremor (Brocker et al., 2013).

In this paper, we propose that the closed-loop nonlinear nonparametric model of hippocampal-entorhinal loop dynamics may be used as a working model to study the effects of DBS on hippocampal seizures. The effects of DBS frequency was analyzed by perturbing the closed-loop model with random narrowband (RNB) spike trains across a wide range of frequencies. It was found that while certain frequencies such as high theta/alpha (4-12 Hz) dramatically increased hippocampal output, other frequencies such as delta (<2 Hz) and low gamma (30Hz) significantly reduced output (see Fig. 12). Furthermore, it was found that depending on the oscillation frequency, the advocated RNB trains may be more efficacious than random (Poisson) trains. Although our model is still in the proof-of-concept stage, it may already help explain some unresolved phenomena seen in experimental studies. First, it is well known that some frequencies initiate seizures while others suppress them. For example in the rodent thalamus, low-frequency stimulation (LFS) at 8 Hz induces seizures, while high-frequency stimulation (HFS) at 100 Hz suppresses them (Mirski et al., 1997); conversely, in the human caudate nucleus, 4-6 Hz LFS suppresses seizures, while 50-100 Hz HFS stimulation induces them (Chkhenkeli and Chkhenkeli, 1997). Furthermore, it has been shown that vastly different stimulation frequencies may suppress seizures in the same system. For example, Kinoshita et al. (2005) showed that both 1 Hz and 50 Hz stimulation had anticonvulsant effects in TLE. Our results suggest that these seemingly disparate multiphasic effects of neurostimulation arise from the closed-loop dynamical interaction between the various regions of the hippocampal-entorhinal circuit, and in such a circuit it is expected to see multiple resonant modes and multiple inhibitory zones. Thus, we suggest that the closed-loop modeling methodology advocated here may be used to understand these complex interactions and obtain efficient DBS patterns to abate seizures.

However, we emphasize that while the presented paradigm of model-based neurostimulation is promising, the specific results should not be taken overly literally. For example, although in our model 30 Hz gamma stimulation was found to be optimal, we cannot yet be certain

whether this is an inherent feature of rodent hippocampal circuitry, or was specific to the particular circuitry of the given rodent during the behavioral task from which the data was obtained. Furthermore, our model says nothing of how stimulation of any other area such as the thalamus would affect the hippocampus. Nonetheless, we believe the model-based approach, if carefully applied, can answer all these questions.

In the current study, MFR was used as a measure of seizure activity. In the future, we hope to expand our model by incorporating multiple units and LFP recordings. This would allow our model to utilize much more realistic indicators of seizure activity than MFR such as population synchrony and field potential oscillations. Also, we hope to provide experimental validation to the computational results obtained here.

acknowledgements

This work was supported by NIH grant P41-EB001978 to the Biomedical Simulations Resource at the University of Southern California and DARPA contract N66601-09-C-2081.

References

Alonso A, Garcia-Austt E. Neuronal sources of theta rhythm in the entorhinal cortex of the rat. Experimental brain research. 1987; 67(3):493–501. [PubMed: 3653311]

Axmacher, Nikolai; Mormann, Florian; Fernández, Guillen; Elger, Christian E.; Fell, Juergen. Memory formation by neuronal synchronization. Brain research reviews. 2006; 52(1):170–182. [PubMed: 16545463]

Barbarosie, Michaela; Avoli, Massimo. Ca3-driven hippocampal-entorhinal loop controls rather than sustains in vitro limbic seizures. The Journal of neuroscience. 1997; 17(23):9308–9314. [PubMed: 9364076]

Bartesaghi R, Migliore M, Gessi T. Input-output relations in the entorhinal cortex-dentate-hippocampal system: evidence for a non-linear transfer of signals. Neuroscience. 2006; 142(1):247–265. [PubMed: 16844310]

Bartesaghi, Renata; Gessi, Tiziana. Activation of perforant path neurons to field ca1 by hippocampal projections. Hippocampus. 2003; 13(2):235–249. [PubMed: 12699331]

Begley, Charles E.; Famulari, Melissa; Annegers, John F.; Lairson, David R.; Reynolds, Thomas F.; Coan, Sharon; Dubinsky, Stephanie; Newmark, Michael E.; Leibson, Cynthia; So, EL. The cost of epilepsy in the united states: An estimate from population-based clinical and survey data. Epilepsia. 2000; 41(3):342–351. others. [PubMed: 10714408]

Ben-Menachem, Elinor; Krauss, Gregory L. Epilepsy: Responsive neurostimulation [mdash] modulating the epileptic brain. Nature Reviews Neurology. 2014

Berger, Theodore W.; Song, Dong; Chan, Rosa HM.; Marmarelis, Vasilis Z.; La-Coss, Jeff; Wills, Jack; Hampson, Robert E.; Deadwyler, Sam A.; Granacki, John J. A hippocampal cognitive prosthesis: multi-input, multi-output non-linear modeling and vlsi implementation. Neural Systems and Rehabilitation Engineering, IEEE Transactions on. 2012; 20(2):198–211.

Boido, Davide; Jesuthasan, Nithiya; de Curtis, Marco; Uva, Laura. Network dynamics during the progression of seizure-like events in the hippocampal-parahippocampal regions. Cerebral Cortex. 2014; 24(1):163–173. [PubMed: 23048021]

Bragin A, Csicsvari J, Penttonen M, Buzsaki G. Epileptic afterdischarge in the hippocampal-entorhinal system: current source density and unit studies. Neuroscience. 1997; 76(4):1187–1203. [PubMed: 9027878]

Brocker, David T.; Swan, Brandon D.; Turner, Dennis A.; Gross, Robert E.; Tatter, Stephen B.; Koop, Mandy Miller; Bronte-Stewart, Helen; Grill, Warren M. Improved efficacy of temporally non-regular deep brain stimulation in parkinson's disease. Experimental neurology. 2013; 239:60–67. [PubMed: 23022917]

Brodie, Martin J.; Dichter, Marc A. Antiepileptic drugs. New England Journal of Medicine. 1996; 334(3):168–175. [PubMed: 8531974]

Buffel, Ine; Meurs, Alfred; Raedt, Robrecht; De Herdt, Veerle; Decorte, Leen; Bertier, Laurence; Delbeke, Jean; Wadman, Wytse; Vonck, Kristl; Boon, Paul. The effect of high and low frequency cortical stimulation with a fixed or a poisson distributed interpulse interval on cortical excitability in rats. International journal of neural systems. 2014; 24(02):1430005. [PubMed: 24475897]

Buzsáki, Gy. Two-stage model of memory trace formation: a role for “noisy” brain states. Neuroscience. 1989; 31(3):551–570. [PubMed: 2687720]

Buzsáki, György. The hippocampo-neocortical dialogue. Cerebral Cortex. 1996; 6(2):81–92. [PubMed: 8670641]

Buzsáki, György. Theta oscillations in the hippocampus. Neuron. 2002; 33(3):325–340. [PubMed: 11832222]

Buzsáki, György; Moser, Edvard I. Memory, navigation and theta rhythm in the hippocampal-entorhinal system. Nature neuroscience. 2013; 16(2):130–138. [PubMed: 23354386]

Chkhenkeli SA, Chkhenkeli IS. Effects of therapeutic stimulation of nucleus caudatus on epileptic electrical activity of brain in patients with intractable epilepsy. Stereotactic and functional neurosurgery. 1997; 69(1-4):221–224. [PubMed: 9711758]

Colgin, Laura Lee. Mechanisms and functions of theta rhythms. Annual review of neuroscience. 2013; 36:295–312.

Colom, Luis V. Septal networks: relevance to theta rhythm, epilepsy and alzheimer's disease. Journal of neurochemistry. 2006; 96(3):609–623. [PubMed: 16405497]

Craig, Sarah; Commins, Sean. Interaction between paired-pulse facilitation and long-term potentiation in the projection from hippocampal area ca1 to the entorhinal cortex. Neuroscience research. 2005; 53(2):140–146. [PubMed: 16039740]

Deadwyler, Sam A.; West, James R.; Cotman, Carl W.; Lynch, Gary. Physiological studies of the reciprocal connections between the hippocampus and entorhinal cortex. Experimental neurology. 1975; 49(1):35–57. [PubMed: 171171]

Durand, Dominique M.; Bikson, Marom. Suppression and control of epileptiform activity by electrical stimulation: a review. Proceedings of the IEEE. 2001; 89(7):1065–1082.

Eikenberry, Steffen E.; Marmarelis, Vasilis Z. A nonlinear autoregressive volterra model of the hodgkin-huxley equations. Journal of computational neuroscience. 2013; 34(1):163–183. [PubMed: 22878687]

Engel, Jerome; Wiebe, Samuel; French, Jacqueline; Sperling, Michael; Williamson, Peter; Spencer, Dennis; Gumnit, Robert; Zahn, Catherine; West-brook, Edward; Enos, Bruce. Practice parameter: Temporal lobe and localized neocortical resections for epilepsy report of the quality standards subcommittee of the american academy of neurology, in association with the american epilepsy society and the american association of neurological surgeons. Neurology. 2003; 60(4):538–547. [PubMed: 12601090]

Ezrokhi VL, Kas'yanov AM, Markevich VA, Balaban PM. Reverberation of excitation in living “hippocampal formation-entorhinal cortex” slices from rats. optical recording. Neuroscience and behavioral physiology. 2001; 31(1):31–37. [PubMed: 11265811]

Finch, David M.; Wong, Ernest E.; Derian, Edie L.; Babb, Thomas L. Neuro-physiology of limbic system pathways in the rat: projections from the subicular complex and hippocampus to the entorhinal cortex. Brain research. 1986; 397(2):205–213. [PubMed: 3542119]

Fisher, Robert S.; Velasco, Ana Luisa. Electrical brain stimulation for epilepsy. Nature Reviews Neurology. 2014

Fricker, Desdemona; Verheugen, Jos AH.; Miles, Richard. Cell-attached measurements of the firing threshold of rat hippocampal neurones. The Journal of Physiology. 1999; 517(3):791–804. [PubMed: 10358119]

Fuster, Joaquin M. Cortical dynamics of memory. International Journal of Psychophysiology. 2000; 35(2):155–164. [PubMed: 10677644]

Goutagny, Romain; Jackson, Jesse; Williams, Sylvain. Self-generated theta oscillations in the hippocampus. Nature neuroscience. 2009; 12(12)

Grill, Warren M.; Brocker, David T.; Kent, Alexander R. Devices, systems and methods for deep brain stimulation parameters. Nov. 2014 US Patent 20,140,350,634

Haas, Julie S.; White, John A. Frequency selectivity of layer ii stellate cells in the medial entorhinal cortex. Journal of neurophysiology. 2002; 88(5):2422–2429. [PubMed: 12424283]

Hampson, Robert E.; Gerhardt, Greg A.; Marmarelis, Vasilis; Song, Dong; Opris, Ioan; Santos, Lucas; Berger, Theodore W.; Deadwyler, Sam A. Facilitation and restoration of cognitive function in primate prefrontal cortex by a neuroprosthesis that utilizes minicolumn-specific neural firing. Journal of neural engineering. 2012; 9(5):056012. [PubMed: 22976769]

Hanley, James A.; McNeil, Barbara J. The meaning and use of the area under a receiver operating characteristic (roc) curve. Radiology. 1982:29–36. [PubMed: 7063747]

Hebb, Donald Olding. The organization of behavior: A neuropsychological theory. Psychology Press; 1949.

Heck, Christianne N.; King-Stephens, David; Massey, Andrew D.; Nair, Dileep R.; Jobst, Barbara C.; Barkley, Gregory L.; Salanova, Vicenta; Cole, Andrew J.; Smith, Michael C.; Gwinn, Ryder P. Two-year seizure reduction in adults with medically intractable partial onset epilepsy treated with responsive neurostimulation: Final results of the rns system pivotal trial. Epilepsia. 2014; 55(3): 432–441. others. [PubMed: 24621228]

Holt, Abbey B.; Netoff, Theoden I. Origins and suppression of oscillations in a computational model of parkinson's disease. Journal of computational neuroscience. 2014; 37(3):505–521. [PubMed: 25099916]

Hutcheon, Bruce; Yarom, Yosef. Resonance, oscillation and the intrinsic frequency preferences of neurons. Trends in neurosciences. 2000; 23(5):216–222. [PubMed: 10782127]

Iijima, Toshio; Witter, Menno P.; Ichikawa, Michinori; Tominaga, Takashi; Kajiwara, Riichi. Matsumoto, Gen. Entorhinal-hippocampal interactions revealed by real-time imaging. Science. 1996; 272(5265):1176–1179. [PubMed: 8638163]

Jahnsen, Henrik; Karnup, Sergei. A spectral analysis of the integration of artificial synaptic potentials in mammalian central neurons. Brain research. 1994; 666(1):9–20. [PubMed: 7889372]

Jones, Roland SG. Entorhinal-hippocampal connections: a speculative view of their function. Trends in neurosciences. 1993; 16(2):58–64. [PubMed: 7680501]

Kinoshita, Masako; Ikeda, Akio; Matsuhashi, Masao; Matsumoto, Riki; Hitomi, Takefumi; Begum, Tahamina; Usui, Keiko; Takayama, Motohiro; Mikuni, Nobuhiro; Miyamoto, Susumu. Electric cortical stimulation suppresses epileptic and background activities in neocortical epilepsy and mesial temporal lobe epilepsy. Clinical neurophysiology. 2005; 116(6):1291–1299. others. [PubMed: 15978492]

Kloosterman, Fabian; van Haeften, Theo; Lopes da Silva, Fernando H. Two reentrant pathways in the hippocampal-entorhinal system. Hippocampus. 2004; 14(8):1026–1039. [PubMed: 15390170]

Kocsis, Bernat; Bragin, Anatol; Buzsáki, György. Interdependence of multiple theta generators in the hippocampus: a partial coherence analysis. The Journal of neuroscience. 1999; 19(14):6200–6212. [PubMed: 10407056]

Leung, L Stan; Yu, Hui-Wen. Theta-frequency resonance in hippocampal ca1 neurons in vitro demonstrated by sinusoidal current injection. Journal of neurophysiology. 1998; 79(3):1592–1596. [PubMed: 9497437]

Lu, Ude; Roach, Shane M.; Song, Dong; Berger, Theodore W. Nonlinear dynamic modeling of neuron action potential threshold during synaptically driven broadband intracellular activity. Biomedical Engineering, IEEE Trans-actions on. 2012; 59(3):706–716.

Marmarelis, Vasilis Z. Nonlinear dynamic modeling of physiological systems. Wiley-Interscience; 2004.

Marmarelis, Vasilis Z.; Zanos, Theodoros P.; Berger, Theodore W. Boolean modeling of neural systems with point-process inputs and outputs. part i: Theory and simulations. Annals of biomedical engineering. 2009; 37(8):1654–1667. [PubMed: 19517238]

Marmarelis, Vasilis Z.; Shin, Dae C.; Song, Dong; Hampson, Robert E.; Deadwyler, Sam A.; Berger, Theodore W. Nonlinear modeling of dynamic interactions within neuronal ensembles using principal dynamic modes. Journal of computational neuroscience. 2013a; 34(1):73–87. [PubMed: 23011343]

Marmarelis, Vasilis Z.; Shin, Dae C.; Song, Dong; Hampson, Robert E.; Deadwyler, Sam A.; Berger, Theodore W. On parsing the neural code in the prefrontal cortex of primates using principal dynamic modes. Journal of computational neuroscience. 2014; 36(3):321–337. [PubMed: 23929124]

Marmarelis VZ, Citron MC, Vivo CP. Minimum-order wiener modelling of spike-output systems. Biological cybernetics. 1986; 54(2):115–123. [PubMed: 3719030]

Marmarelis VZ, Shin DC, Orme ME, Zhang R. Closed-loop dynamic modeling of cerebral hemodynamics. Annals of biomedical engineering. 2013b; 41(5):1029–1048. [PubMed: 23292615]

Mina, Faten; Benquet, Pascal; Pasnicu, Anca; Biraben, Arnaud; Wendling, Fabrice. Modulation of epileptic activity by deep brain stimulation: a model-based study of frequency-dependent effects. Frontiers in computational neuroscience. 2013; 7

Mirski, Marek A.; Rossell, Lisa Ann; Terry, John B.; Fisher, Robert S. Anti-convulsant effect of anterior thalamic high frequency electrical stimulation in the rat. Epilepsy research. 1997; 28(2): 89–100. [PubMed: 9267773]

Nagao T, Alonso A, Avoli M. Epileptiform activity induced by pilocarpine in the rat hippocampal-entorhinal slice preparation. Neuroscience. 1996; 72(2):399–408. [PubMed: 8737410]

Pare D, Llinas R. Role of the hippocampal-entorhinal loop in temporal lobe epilepsy: extra-and intracellular study in the isolated guinea pig brain in vitro. The Journal of neuroscience. 1992; 12(5):1867–1881. others. [PubMed: 1578275]

Pike, Fenella G.; Goddard, Ruth S.; Suckling, Jillian M.; Ganter, Paul; Kasthuri, Narayanan; Paulsen, Ole. Distinct frequency preferences of different types of rat hippocampal neurones in response to oscillatory input currents. The Journal of Physiology. 2000; 529(1):205–213. [PubMed: 11080262]

Sandler, R.; Shin, DC.; Song, D.; Hampson, RE.; Deadwyler, SA.; Berger, TW.; Marmarelis, VZ. Neural Engineering (NER), 2013 6th International IEEE/EMBS Conference on. IEEE; 2013. Closed-loop modeling of the hippocampus and design of neurostimulation patterns for suppressing seizures.; p. 1143-1146.

Sandler, Roman A.; Marmarelis, Vasilis Z. Understanding spike triggered covariance using wiener theory for receptive field identification. Journal of Vision. in press.

Sandler, Roman A.; Song, Dong; Hampson, Robert E.; Deadwyler, Sam A.; Berger, Theodore W.; Marmarelis, Vasilis Z. Model-based asessment of an in-vivo predictive relationship from ca1 to ca3 in the rodent hippocampus. Journal of computational neuroscience. 2014:1–15.

Sandler, Roman A.; Deadwyler, Samuel A.; Hampson, Robert E.; Song, Dong; Berger, Theodore W.; Marmarelis, Vasilis Z. System identification of point-process neural systems using probability based volterra kernels. Journal of neuroscience methods. 2015; 240:179–192. [PubMed: 25479231]

Schreiber, Susanne; Erchova, Irina; Heinemann, Uwe; Herz, Andreas V. Subthreshold resonance explains the frequency-dependent integration of periodic as well as random stimuli in the entorhinal cortex. J Neurophysiol. 2004; 92(1)

Sik, Attila; Ylinen, Aarne; Penttonen, Markku; Buzsaki, Gyorgy. Inhibitory ca1-ca3-hilar region feedback in the hippocampus. Science. 1994; 265(5179):1722–1724. [PubMed: 8085161]

Song, Dong; Chan, Rosa HM.; Marmarelis, Vasilis Z.; Hampson, Robert E.; Dead-wyler, Sam A.; Berger, Theodore W. Nonlinear dynamic modeling of spike train transformations for hippocampal-cortical prostheses. Biomedical Engineering, IEEE Transactions on. 2007; 54(6):1053–1066.

Song, Dong; Chan, Rosa HM.; Marmarelis, Vasilis Z.; Hampson, Robert E.; Dead-wyler, Sam A.; Berger, Theodore W. Nonlinear modeling of neural population dynamics for hippocampal prostheses. Neural Networks. 2009a; 22(9):1340–1351. [PubMed: 19501484]

Song, Dong; Marmarelis, Vasilis Z.; Berger, Theodore W. Parametric and non-parametric modeling of short-term synaptic plasticity. part i: Computational study. Journal of computational neuroscience. 2009b; 26(1):1–19. [PubMed: 18506609]

Song, Dong; Wang, Zhuo; Marmarelis, Vasilis Z.; Berger, Theodore W. Para-metric and non-parametric modeling of short-term synaptic plasticity. part ii: Experimental study. Journal of computational neuroscience. 2009c; 26(1):21–37. [PubMed: 18504530]

Spruston, N.; McBain, C. Structural and functional properties of hippocampal neurons. The hippocampus book; 2007. p. 133-201.

Stringer, Janet L.; Lothman, Eric W. Reverberatory seizure discharges in hippocampal-parahippocampal circuits. Experimental neurology. 1992; 116(2):198–203. [PubMed: 1577127]

Tamamaki, Nobuaki; Nojyo, Yoshiaki. Preservation of topography in the connections between the subiculum, field ca1, and the entorhinal cortex in rats. Journal of Comparative Neurology. 1995; 353(3):379–390. [PubMed: 7538515]

Taylor, Peter Neal; Thomas, Jijju; Sinha, Nishant; Dauwels, Justin; Kaiser, Marcus; Thesen, Thomas; Ruths, Justin. Optimal control based seizure abatement using patient derived connectivity. Frontiers in Neuroscience. 2015; 9:202. [PubMed: 26089775]

Valenza, Gaetano; Citi, Luca; Scilingo, E.; Barbieri, Riccardo. Point-process nonlinear models with laguerre and volterra expansions: instantaneous assessment of heartbeat dynamics. 2013

Van Nieuwenhuyse B, Raedt R, Delbeke J, Wadman WJ, Boon P, Vonck K. In search of optimal dbs paradigms to treat epilepsy: Bilateral versus unilateral hippocampal stimulation in a rat model for temporal lobe epilepsy. Brain stimulation. 2014

Winson, Jonathan. Loss of hippocampal theta rhythm results in spatial memory deficit in the rat. Science. 1978; 201(4351):160–163. [PubMed: 663646]

Wu, Kun; Canning, Kevin J.; Leung, L Stan. Functional interconnections between ca3 and the dentate gyrus revealed by current source density analysis. Hippocampus. 1998; 8(3):217–230. [PubMed: 9662137]

Wyckhuys, Tine; Boon, Paul; Raedt, Robrecht; Van Nieuwenhuyse, Bregt; Vonck, Kristl; Wadman, Wytse. Suppression of hippocampal epileptic seizures in the kainate rat by poisson distributed stimulation. Epilepsia. 2010; 51(11):2297–2304. [PubMed: 20973781]

Yeckel, Mark F.; Berger, Theodore W. Feedforward excitation of the hippocampus by afferents from the entorhinal cortex: redefinition of the role of the trisynaptic pathway. Proceedings of the National Academy of Sciences. 1990; 87(15):5832–5836.

Zanos, Theodoros P.; Courellis, Spiros H.; Berger, Theodore W.; Hampson, Robert E.; Deadwyler, Sam A.; Marmarelis, Vasilis Z. Nonlinear modeling of causal interrelationships in neuronal ensembles. Neural Systems and Rehabilitation Engineering, IEEE Transactions on. 2008; 16(4): 336–352.

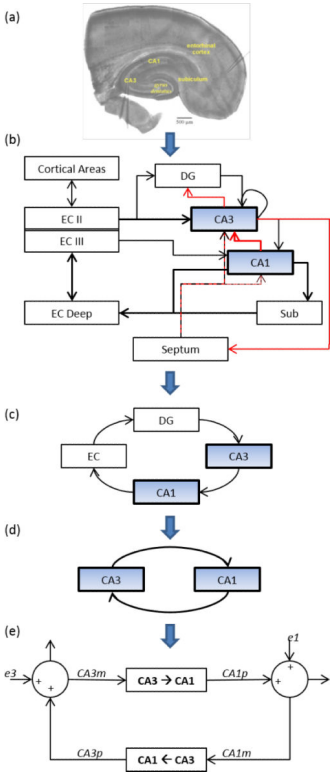

Figure 1.

(A) Horizontal rodent hippocampal slice showing anatomical locations of the areas dealt with in our model. (B) Detailed schematic representation of anatomical connectivity of hippocampus. Black and red lines show excitatory and inhibitory connections, respectively. (C) Schematic of trisynaptic-loop. (D) High level schematic representation of CLPP model. (E) Detailed systems representation of CLPP model

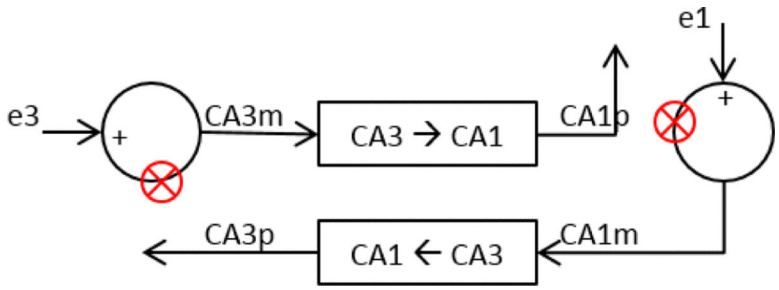

Figure 2.
Open-loop model configuration.

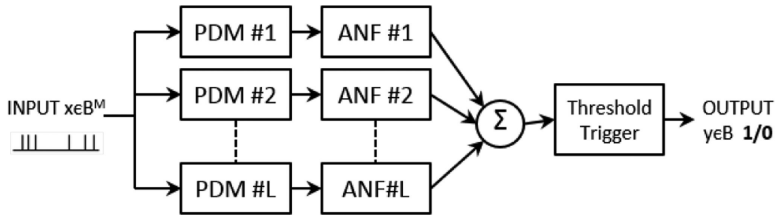

Figure 3.
Volterra-PDM Subsystem Model

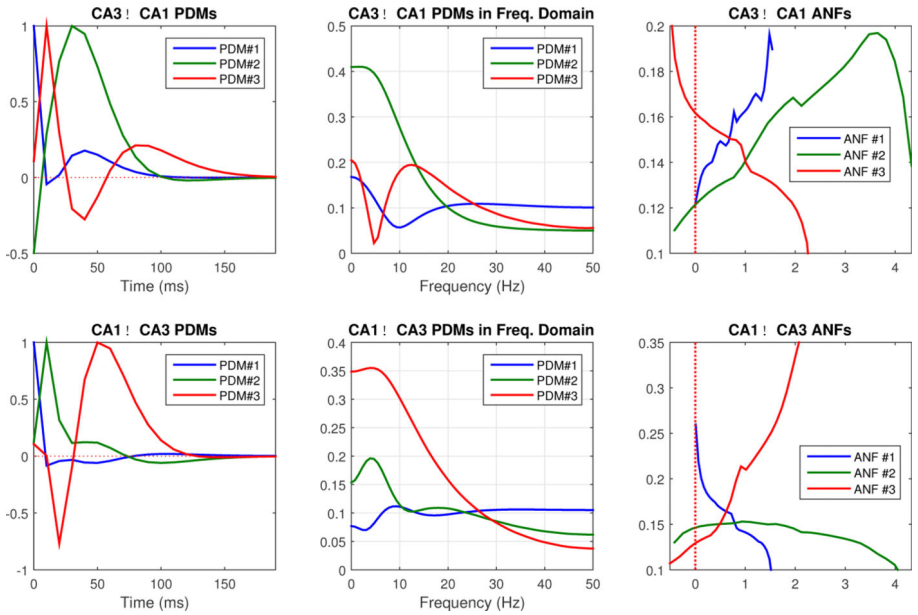

Figure 4.

Obtained Volterra-PDM Subsystems. Top row shows CA3→CA1 subsystem, while bottom row shows that of CA1→CA3. Left column shows PDMs, middle column shows PDMs in frequency domain, and right column shows ANFs. Note that several PDMs have frequency peaks in the theta range.

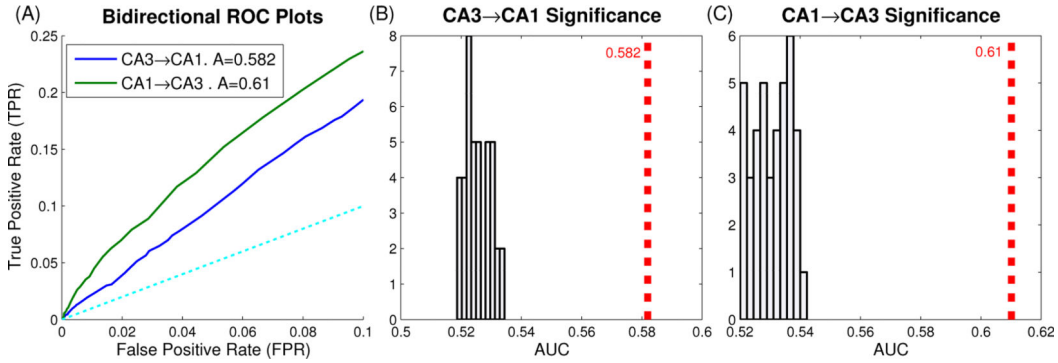

Figure 5.

(A) Bidirectional ROC plots. (B,C) Results of Monte Carlo simulations for CA3→CA1 (B) and CA1→CA3 (C). Histogram plots the predictive power (AUC) of N=40 random inputs with the same MFR as the true input. The AUC of the true input is shown by the dashed red line. In both cases the true AUC was greater than the random AUC's with $P < .0001$

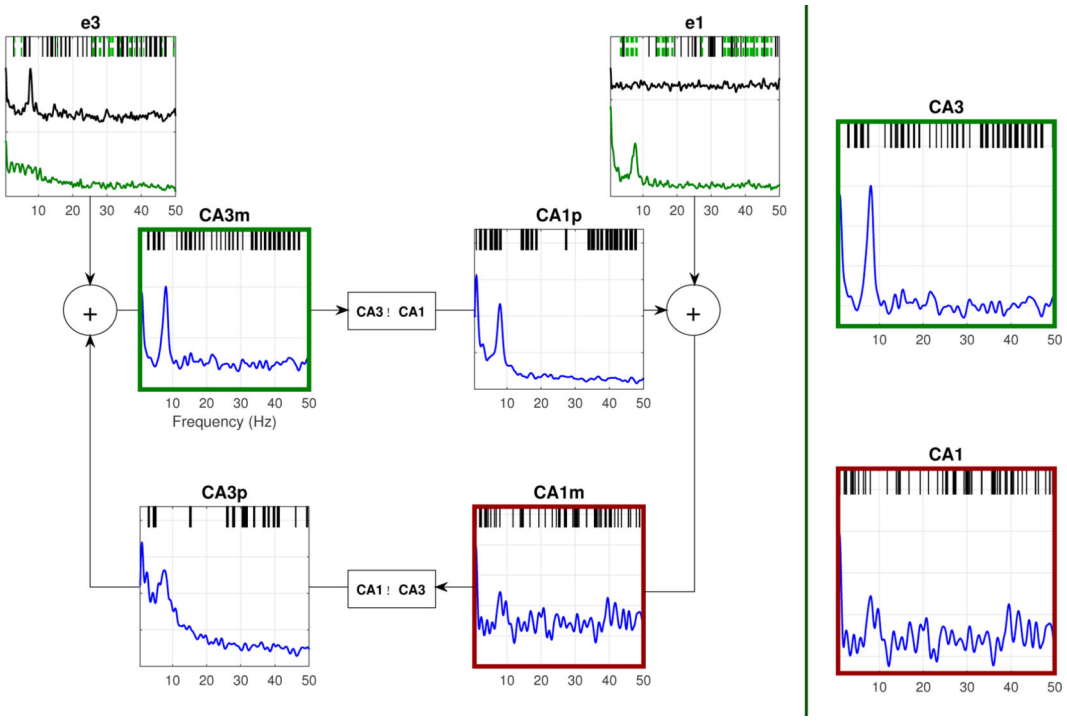

Figure 6.

CLPP System driven by residual input. Each inset shows the given signal in the frequency domain (below) and time domain (above). The time domain rasterplot is a representative sample of the signal spanning 6 seconds. Disturbance signals e1 and e3 are tertiary signals with positive spikes in black and negative spikes in green. Their corresponding spectra are below in the same color. Each frequency-domain plot shows the Fourier transform of the signal, which was then low-passed through a 20 Hz filter and then smoothed to ease visibility.

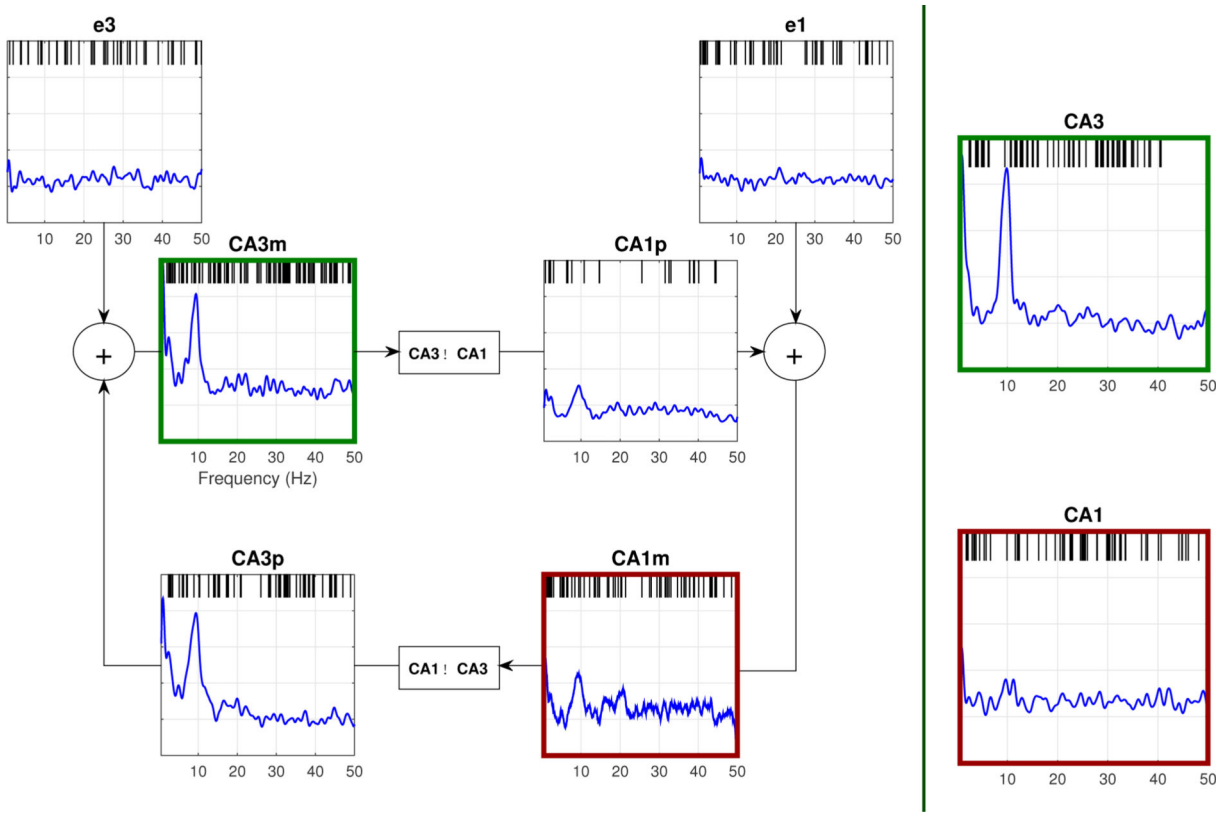

Figure 7.

CLPP Model driven by broadband inputs. Layout is the same as Fig. 6 except that here the exogenous signals e3 and e1 were binary rather than tertiary.

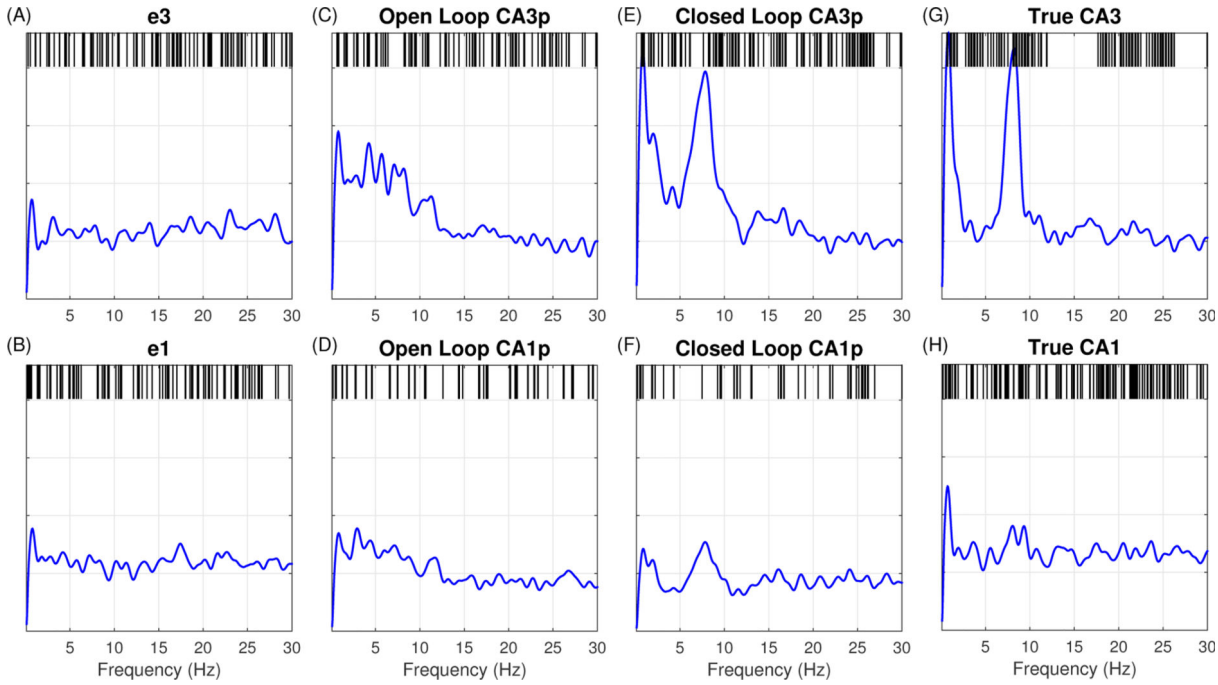

Figure 8.

Comparison of Open-Loop and Closed-Loop systems driven by identical broadband inputs e3 and e1. Note robust theta rhythms only arise in the closed-loop case.

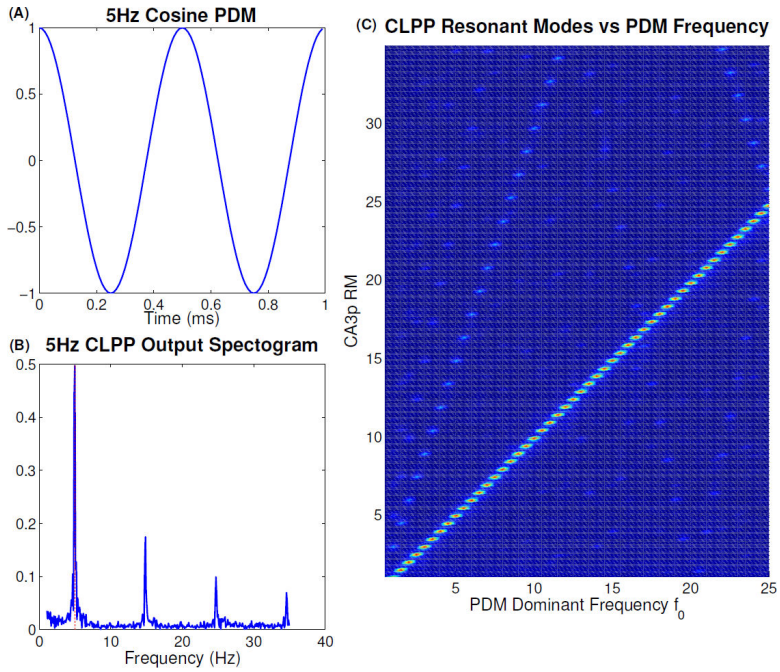

Figure 9.

Analysis of synthetic system showing relationship between PDMs and resonant modes. In this synthetic system, each subsystem is composed of a single cosine PDM of freq f_0=5Hz, shown in (A). The only nonlinearity in each subsystem is the threshold trigger (i.e. no ANFs). (B) Shows the CLPP output signal CA1m. Note the resonant mode at 5Hz (marked by red line) matches f_0 exactly. (C) A plot mapping the CLPP output resonant mode with the PDM spectral peak (f_0). Each vertical column represents the FFT of the CLPP output at the given PDM dominant frequency f_0. Notice that despite the strong nonlinearity of the threshold trigger, the CLPP resonant mode corresponds exactly to the PDM spectral peak. Also note the presence of harmonics at $2*f_0$

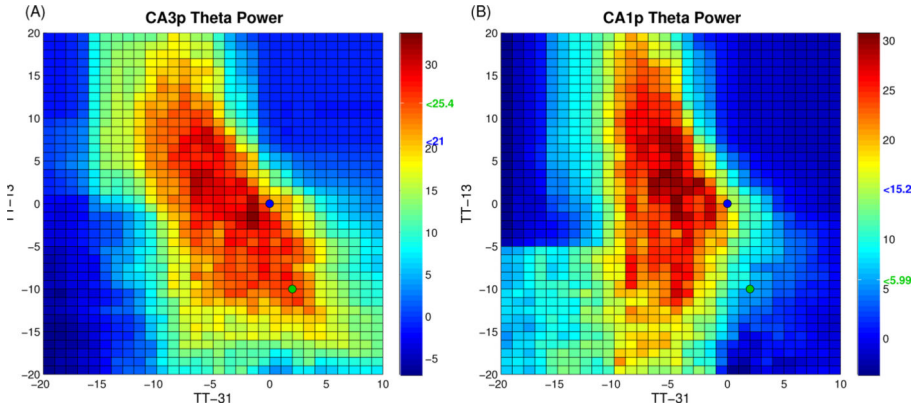

Figure 10.

Effect modifying threshold triggers has on emergent theta resonant modes of CA1p (left) and CA3p (right). X and y axis' measure the percent-change of thresholds from the default threshold (marked by red dot), which is calculated by the methods described previously. Z-axis (color) measures the percent change in the strength of the theta resonant mode as compared to the default case. Each point represents the theta band power in a simulation conducted with the threshold values in the x,y axis and broadband inputs. Identical broadband inputs were used in each simulation. Notice that different threshold combinations favor a stronger theta in either CA3 or CA1, for example by lowering the CA1→CA3 threshold by 10% and raising the CA3→CA1 threshold by 2% (marked by green dot), theta only appears in CA3, as in real data.

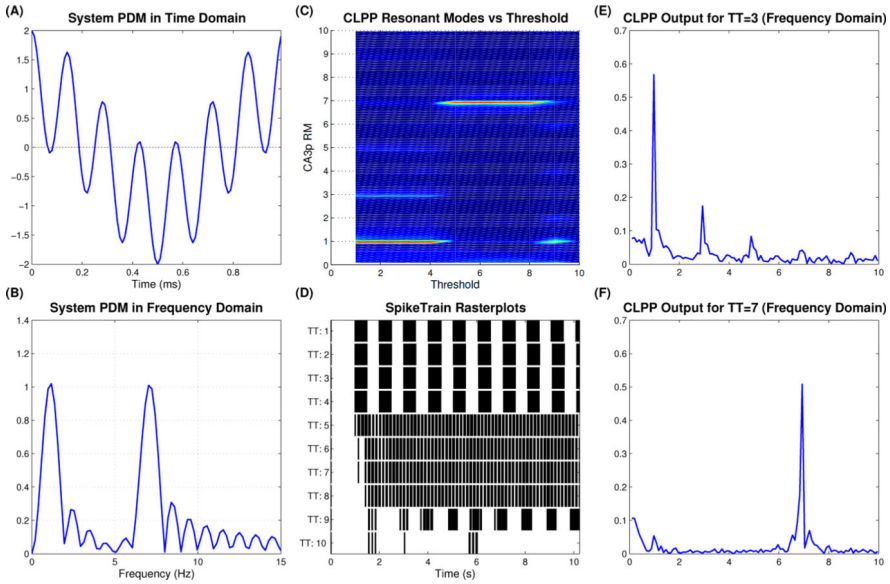

Figure 11.

Effect threshold has on synthetic cosine system. Each subsystem was composed of a single PDM which was the sum of two cosine waves of different frequency. (A) Shows the PDM in the time domain, while (B) shows the PDM in the frequency domain. The only nonlinearity in each subsystem is the threshold trigger (i.e. no ANFs). (C) Effect of changing the threshold trigger on the resonant mode peak power. Plot is the same as Fig. 9C. Notice that the threshold determines which resonant mode will emerge in the CLPP output signals. (D) shows the evolution of the spike train rasterplots as the threshold is changed. (E) and (F) show the CLPP outputs in the frequency domain when the threshold is 3 and 7, respectively.

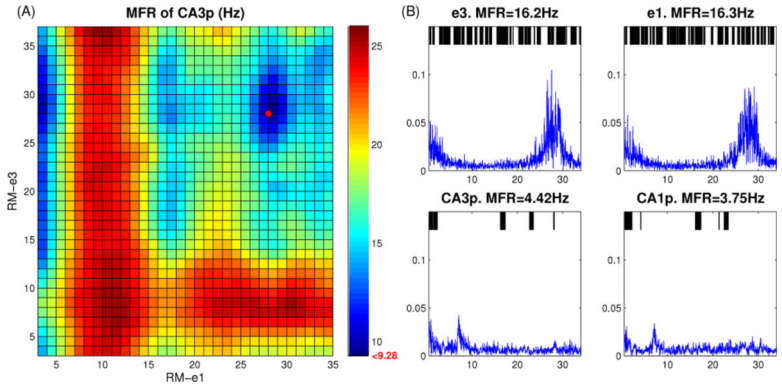

Figure 12.

(A) CA3p output MFR where e3 & e1 are RNB inputs of various frequencies. X and y axis' show the narrowband frequency of e3 and e1 respectively. The x and y value of 0 corresponds to a Poisson input. Note that when the CLPP system is driven by RNB theta inputs (around 8 Hz) system output will greatly increase. When the system is driven by low frequencies or 28 Hz, system output will greatly decrease. (B) example of CLPP driven by two RNB inputs centered at 28 Hz. Note that subsystem output MFR is far less than input MFR.

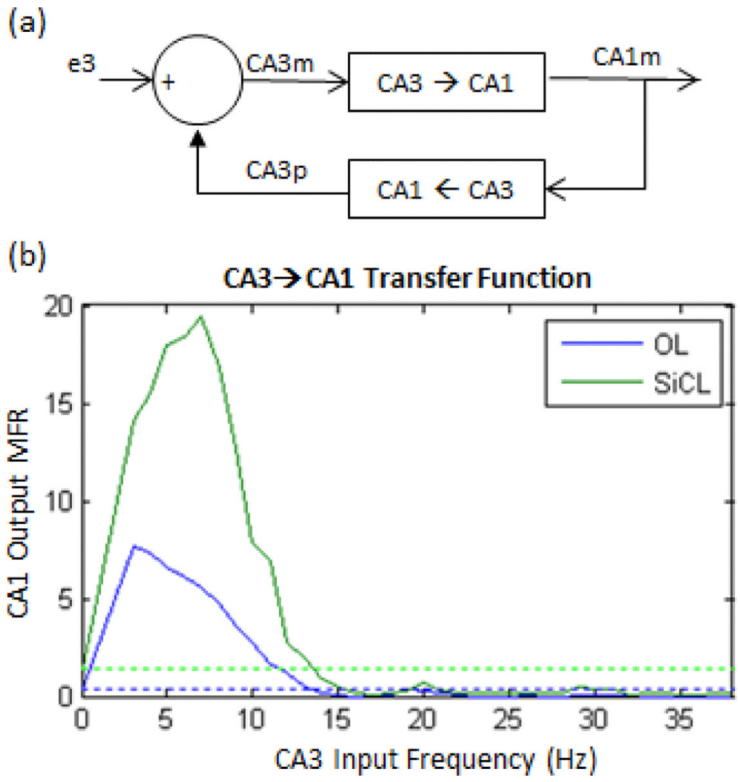

Figure 13.

(A) Schematic of single-input closed-loop model from CA3→CA1. (B) Open-loop (OL) and Single-Input closed loop (SiCL) output MFR responses to RNB inputs of varying frequencies.

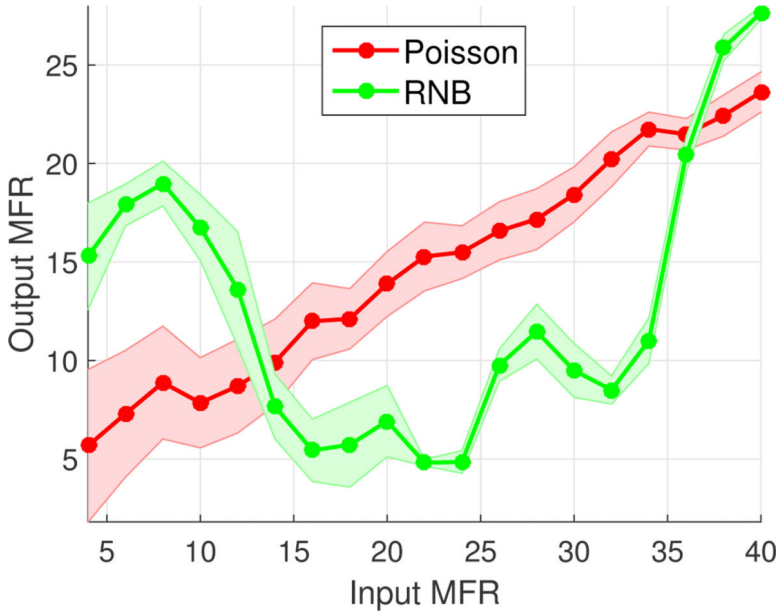

Figure 14.

System output, as measured by MFR of CA1, when stimulated with random and RNB spiketrains of various frequencies. Each trial was conducted 10 times. Lines and shaded region show mean ± standard deviation.